Field Tests of a Three-Span Continuous Highway Bridge

JAMES W. BALDWIN
Associate Professor of Civil Engineering, University of Missouri

A three-span continuous I-beam bridge of non-composite design was subjected to several series of static and dynamic tests. Strains and deflections in each stringer were recorded continuously during the tests. Moments in the bridge were calculated from the experimental strains by taking into account the semi-composite nature of the structure. These moments were compared with those calculated by elastic analysis. Measured deflections were also compared with those predicted by the elastic analysis. The nature of the semi-composite behavior was studied. The friction-link phenomenon provided an explanation of the rather unusual observed behavior. Lateral distributions of moment and deflection were compared with theoretical analyses and with the AASHO code.

Response of the structure to dynamic loads was compared with theoretical analyses and found to be in reasonable agreement. Within the limits of these tests, speed of the test vehicle was found to have only a slight effect on the impact factor. Severe roughness at the approach was found to have little effect on the maximum moments and deflections. Consideration of the damping characteristics of the vehicle suspension indicates that the effects of the roughness were damped out before the vehicle reached a critical position in the span.

THE ACCEPTED design procedure for bridges subject to dynamic loads is based on a static analysis modified by an arbitrary factor called the impact factor. The introduction of new materials coupled with a desire for greater economy in design has resulted in the design of members which are much more flexible than those designed previously. This trend has created the need for a better understanding of the actual behavior of bridges under dynamic loads. Since 1953, the U. S. Bureau of Public Roads, in cooperation with various state highway departments, has conducted field dynamic tests on several highway bridges. The investigation reported herein is the result of such a cooperative undertaking with the Missouri State Highway Department. The test bridge, known as the Burris Fork Bridge, is located on Route 87 about five miles south of California in Moniteau County, Missouri.

Construction of the bridge was completed in July 1954, and the testing was carried out between August 24 and September 30, 1955. Preliminary reduction of the data was carried out by the Missouri State Highway Department and the U. S. Bureau of Public Roads between 1956 and 1960.

The bridge consists of three continuous spans and one simple approach span. A report (1) on the simple approach span was prepared by the Missouri State Highway Department. The analysis in the following report covers only the three continuous spans and was prepared by the Engineering Experiment Station of the University of Missouri between 1961 and 1963. The complete report has been published (13).

Paper sponsored by Committee on Bridges.

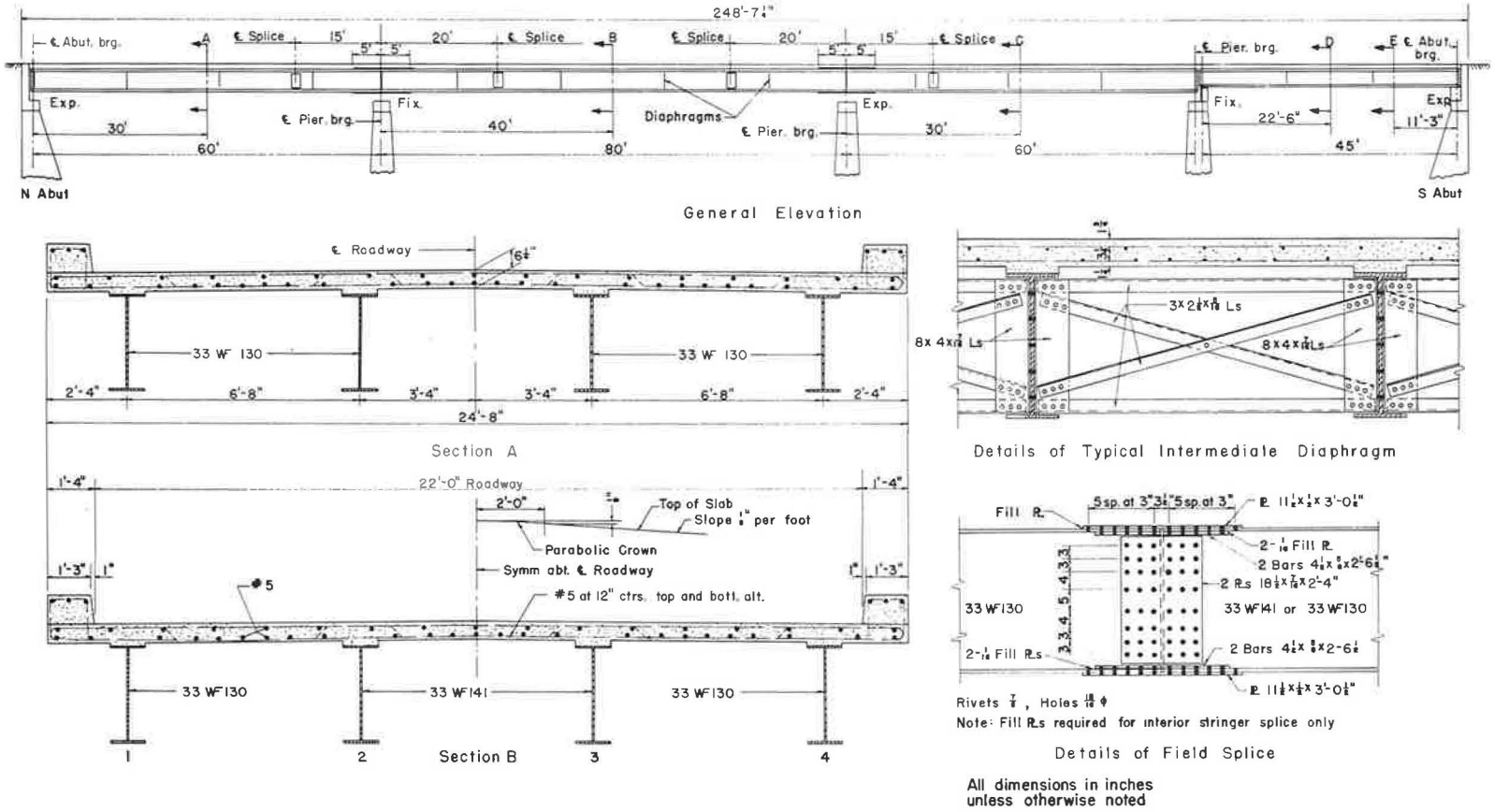

Figure 1. Details of test structure.

EXPERIMENTAL INVESTIGATION

Structure

The three-span test structure is of a non-composite design for H-15-44 loading. Details of the test structure are shown in Figure 1. The 22-ft wide deck is a 6¼-in. reinforced concrete slab supported on four steel I-beam stringers. The stringers are spaced 6 ft 8 in. on centers and consist of 33WF130 or 33WF141 rolled sections (Fig. 1). The 60- by 80- by 60-ft series of continuous bridge spans is supported on three dumbbell-type concrete piers and one open-type concrete end bent, all founded on rock. A photograph of the bridge site is shown in Figure 2.

Test Vehicle

The test vehicle (Fig. 3) was a standard commercial semitrailer truck loaded with gravel to produce approximately the AASHO H20-S16-44 truck loading. Wheel loading and axle spacing of the test vehicle are shown in Figure 4. Spring constants were 5.94 kips/in. for the driver axle and 16.5 kips/in. for the pair of tandem axles.

Instrumentation

Instrumentation was furnished, installed, and operated by the U. S. Bureau of Public Roads. The gages consisted of GE magnetic reluctance gages, SR-4 strain gages, and

Figure 2. Bridge site.

Figure 3. Test vehicle.

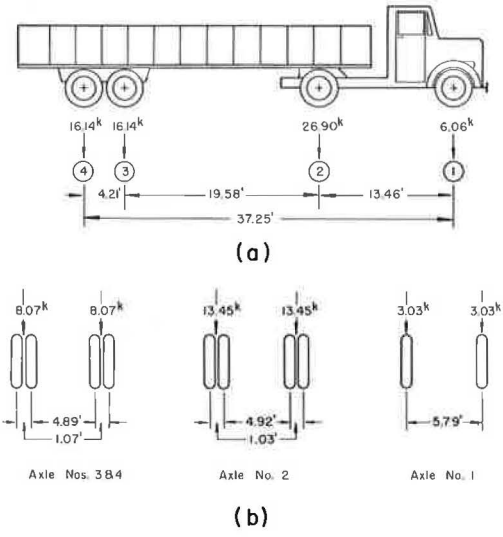

Figure 4. Details of test vehicle: (a) axle spacing and loading, and (b) wheel spacing and loading.

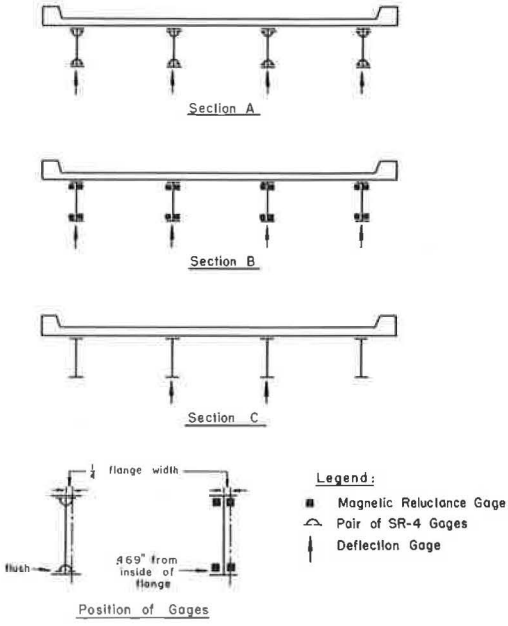

Figure 5. Instrumentation.

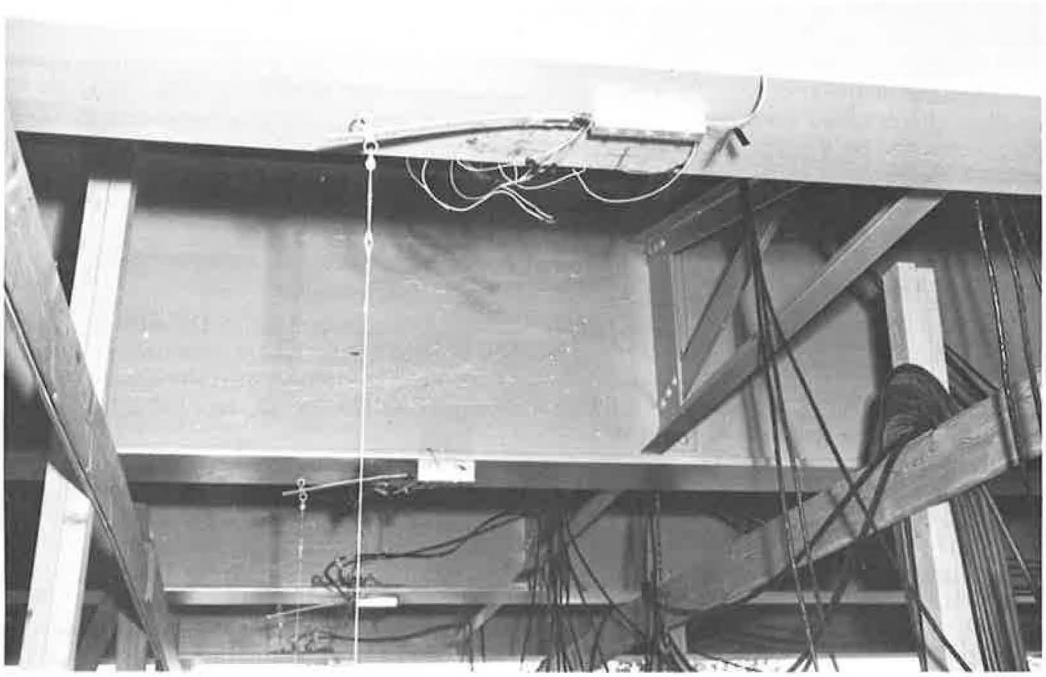

Figure 6. Deflection gages.

deflection gages located as shown in Figure 5. After carefully locating each gage position, paint and mill scale were removed from the steel beams. Resistance-type gages were attached to the structural steel members with a gage cement after the base metal was cleansed with a solvent. Reluctance-type gages were mechanically fastened to the bridge members which required drilling and tapping holes for the attaching screws. In this case the surface of the steel was faced to provide for proper seating of the gages.

Prior to mounting on the bridge the electromagnetic strain gages were calibrated in a test frame by varying the air gap in known increments with a micrometer screw. Since the calibration curves were not exactly linear, care was taken to reestablish the calibration zero position when the gages were attached to the test member.

Deflection gages consisted of SR-4 strain gages mounted on 12-in. aluminum cantilevers as shown in Figure 6. The free end of the cantilever was initially given a deflection greater than that expected in the beam and was fastened to a ground anchor by a light steel cable. Hence, the cable was in tension at all times during the test. Laboratory calibration curves were used to convert the strain-gage signals to deflections.

Four conductor shielded cables were used to connect the gages to the recording equipment which was located in an 18-ft housetrailer. Each gage when connected became one active leg of a Wheatstone bridge circuit. To complete the circuit, dummy gages of each type used were attached to small pieces of structural steel and located near the active gages for temperature compensation. The Wheatstone bridge circuits were arranged in groups of 8 or 12. Each group was energized by a 10-volt 3,000-cycle signal from one oscillator and the modulated return signals from the active gages were fed through individual amplifiers into the recording galvanometers of an oscillograph. There were two oscillographs, each capable of recording 18 signals simultaneously on a 7-in. wide strip of sensitized paper. Circuits were incorporated in each amplifier for calibrating an active variable-resistance gage, balancing the Wheatstone bridge, and regulating the amplifier output.

Additional information on the oscillograph records consisted of record identification numbers, axle position indicators, and 0.1- or 0.01-sec timing lines. The axle position indicators were triggered by air tubes laid across the bridge. The inside of the trailer is shown in Figure 7.

In addition to the instrumentation on the bridge, SR-4 gages were mounted on the axle housing of the truck. The purpose of these gages was to provide a qualitative indication of the force transmitted to the bridge by the truck. Signals from these gages were recorded by a direct writing Brush recorder mounted on the truck. As the truck entered the span, a switch on the underside of the truck was triggered by a flexible obstruction on the bridge. This switch triggered the event marker on the oscillograph, thus indicating the time at which the truck entered the span.

Test Procedure

The bridge was subjected to five series of tests, designated as 1a through 1e. Series 1a, 1b, and 1c were designed to investigate the effects of the lateral position of the truck lane on the bridge. The center of the truck lane coincided with the centerline of the bridge for Series 1a, was 6 ft east of the centerline for Series 1b, and 3 ft east of the centerline for Series 1c.

Series 1d and 1e were designed for the study of induced roughness. In Series 1d the centerline of the truck lane coincided with the centerline of the bridge and the east wheels passed through a 3-in. deep by 5-ft long trench at the north approach to the bridge. In Series 1e, the centerline of the truck lane coincided with the centerline of the bridge and both the east and west wheels passed through trenches at the north approach.

Each series consisted of several static and dynamic test runs. A static test run consisted of taking oscillograph readings from each of the gages with the truck remaining at rest in some position on the bridge. The truck was moved forward in increments of 4 ft between static runs. A dynamic run was conducted by making a continuous recording of each of the gage signals while the truck was driven at a constant rate of speed from one end of the bridge to the other. Nominal truck speeds ranged from 5 to

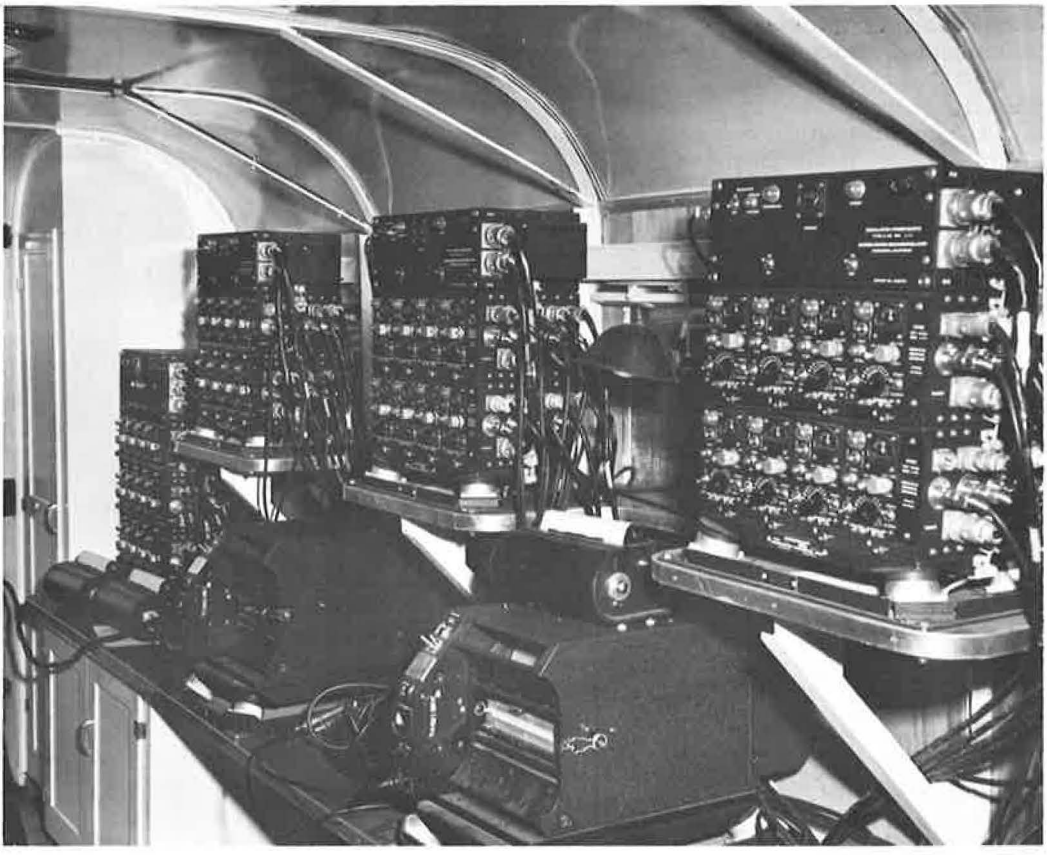

Figure 7. Recording equipment.

TABLE 1

TEST PROGRAM

Series	Displacement[a] (ft)	Static Runs		Dynamic Runs	
		NB	SB	NB	SB
1a	0	6	25	21	21
1b	6[b]	15	24	14	14
1c	3[b]	—	—	6	6
1d	0	—	—	—	10
1e	0	14	—	—	6

[a]Of truck lane from bridge centerline.
[b]East.

50 mph in 5-mph increments. In most cases two runs were made at each speed. A summary of the test program is given in Table 1.

During test runs, the recording equipment was operated through a remote control cable by the engineer on the bridge who also directed the test vehicle operation. Another engineer in the trailer observed the results on the screens of the oscillographs and made adjustments to the equipment when necessary.

Data

The tests described in the previous section resulted in several hundred feet of oscillograph records, each with 18 traces. Three typical oscillograph traces are shown in Figure 8. Because the truck was traveling at a constant rate of speed, the abscissa, time after the driver axle crossed the first support, determines the position of the truck on the bridge. The general shape of the trace is that for an influence line of the particular quantity being measured. In the cases shown in Figure 8, the quantity being measured was the stress in the bottom flange of an interior stringer in Span A. As the truck entered Span A from the north, the stress increased in the positive direction, reaching a maximum when the truck was somewhere near the center of Span A. As the truck proceeded into Span B, the stress became negative, reaching a maximum negative value when the truck was near the center of Span B. The stress reached another positive maximum as the truck passed through Span C.

A smooth curve through the trace (Fig. 8) is referred to as the mean curve, which is modulated by the vibration of the bridge. Thus, the bridge vibration is represented by the higher frequency, lower amplitude wave superimposed on this mean curve. The maximum curve is the outer envelope of the vibration as shown. Actually there are some other differences between the static influence line and the dynamic response not apparent from a cursory examination. These include phase shift and possibly some difference in amplitude.

For the remainder of the discussion the term mean will refer to the maximum value of the mean curve with the vehicle in a particular span; the term maximum will refer to the maximum value of the outer envelope with the vehicle in a particular span.

The first step in the reduction of the data was carried out by the State Highway Department and the U. S. Bureau of Public Roads. The critical ordinates shown in Figure 8

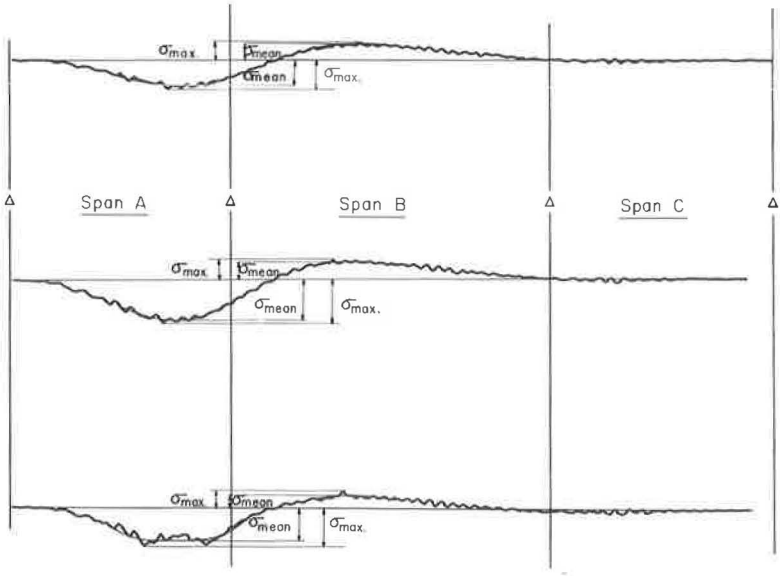

Figure 8. Typical oscillograph traces.

were taken off the oscillograph records. Stress or deflection conversion factors obtained from calibration curves were then used to convert these ordinates to stresses or deflections. The modulus of elasticity for the steel was assumed to be 30×10^6 psi. For each trace of each dynamic run, there was one maximum and one mean value as the truck passed through each span, making a total of six critical quantities for each trace of each run. (Benson-Lehner equipment was used by the U. S. Bureau of Public Roads for their part of the take-off work.) A slight variation in procedure was necessary because the maximum stress in the top flange did not necessarily occur at the same instant as the maximum stress in the bottom flange. To obtain simultaneous values, the stress in the top flange at the instant the stress in the bottom flange reached its maximum value was recorded as the maximum stress in the top flange. Take-off of the static data was much less complicated. A static trace was merely a short straight line representing a constant value.

This initial take-off resulted in approximately 20,000 pieces of data. It was decided that the use of punched cards and a high-speed digital computer would be the most economical method for handling such a large quantity of data. Consequently, the data were immediately punched on cards and all subsequent processing was done by machine. A straight-line extrapolation was used in computing the extreme fiber stresses from stresses at the gage locations.

ANALYSIS OF TEST RESULTS

Comparison of Experiments with Theory

The main objective of the investigation was to compare the experimental results with existing theory. To make satisfactory comparisons, experimental quantities must be compared with realistic theoretical quantities. Design stresses and deflections for the bridge under consideration are not satisfactory for comparison because the design was based on two H-15-44 loads, whereas the test conditions included only one H-20-S16-44 load. In a structure such as a bridge, the situation is complicated even further because several steps are involved in computing stresses for a given loading. First, the impact factor is applied to the load to account for the dynamic effects; next, the load is distributed to the stringers either through a rather complex analysis or by the use of a set of design coefficients. Moments in the stringers are then computed on the basis of elastic theory. Finally, the stresses in the stringers are computed on the basis of either a composite or non-composite section, depending on the type of construction. Completely non-composite action is never realized because the friction between the slab and the stringer always results in some degree of composite action. From a design standpoint, the assumption of completely non-composite action is conservative, whereas from a research standpoint this assumption introduces considerable difference between the experimental and theoretical values.

In comparing experiments with theory, it is desirable to separate the effects of these individual assumptions to determine which are satisfactory and which introduce error into the computations. The analyses in this report were performed in such a manner as to isolate as many individual effects as possible. This was accomplished as follows:

1. The static analysis was first compared with results from static tests, thereby eliminating the unknown effect of impact from the comparison.
2. Forces were compared on the basis of moment rather than stress to eliminate the uncertainties arising from the semi-composite action.
3. The uncertainties arising from lateral distribution were eliminated from these comparisons by considering the total moment in the entire cross-section of the bridge rather than that in a single stringer.
4. Average observed deflections for a given bridge section were compared with computed values for both composite and non-composite analyses.
5. The degree of composite action was evaluated in terms of effective section modulus.
6. Lateral distribution was compared directly with existing theory. Experimental moments were superimposed to produce a two-lane loading for comparison with the AASHO code provisions.

7. Base values for computing impact factors were determined from normalized plots of mean moment and mean deflection vs speed.

There was much scatter in the data where the readings were very small. This was almost always true when the gages were in an unloaded span. Values for Stringers 1 and 2 of Series 1b and 1c were also subject to this difficulty. Consequently, these data were not used in the analysis unless otherwise indicated.

Theoretical Moments

Conventional elastic theory was used in preparing influence lines for moments at Sections A and B due to a unit load passing across the bridge. Separate influence lines were prepared for the interior and exterior stringers. In each case completely non-composite action was assumed. The difference between the influence ordinates of the interior and exterior stringers was never more than 4 or 5 percent. As a result, it was decided that an influence line representing the average of the influence lines for an interior and an exterior stringer could be used satisfactorily as an influence line for

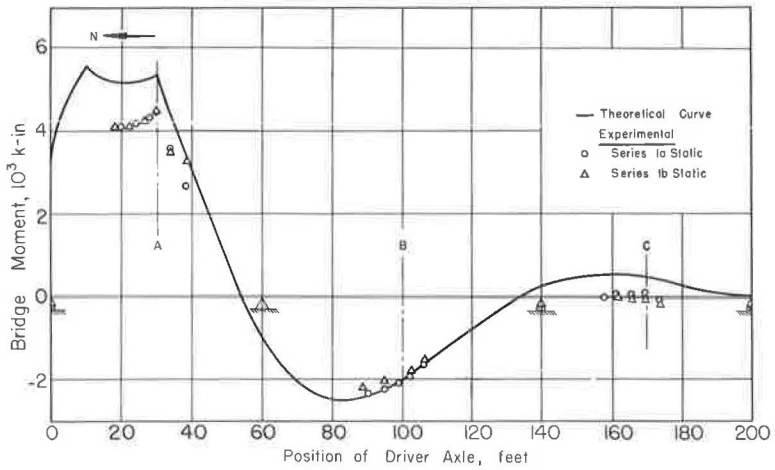

Figure 9. Influence line for bridge moment at Section A, truck northbound.

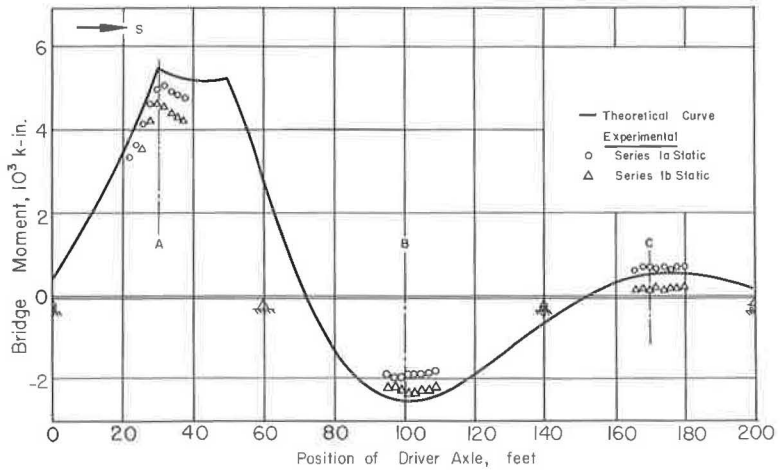

Figure 10. Influence line for bridge moment at Section A, truck southbound.

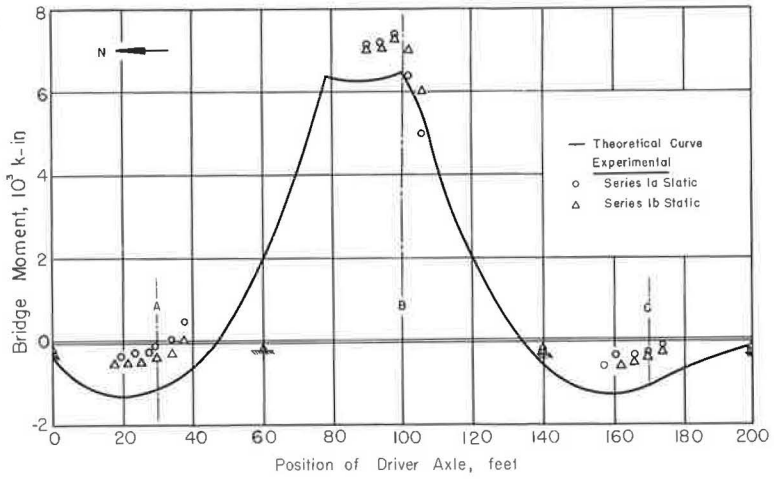

Figure 11. Influence line for bridge moment at Section B, truck northbound.

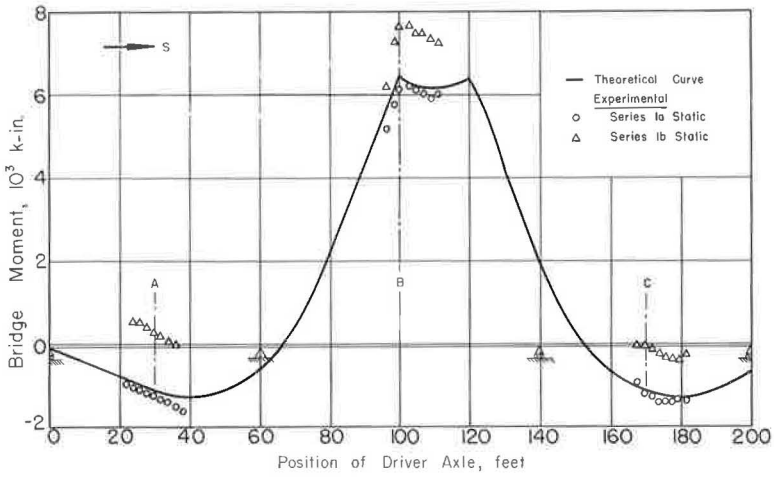

Figure 12. Influence line for bridge moment at Section B, truck southbound.

the entire bridge cross-section. Since such an influence line depends only on the ratios of the moments of inertia at various sections and not on the magnitude of the moment of inertia, these influence lines would be changed only a small amount by considering completely composite action.

Influence lines were then prepared for moments in the bridge at Sections A and B due to the test vehicle. This was accomplished by superimposing influence lines for the front axle, the driver axle, and the tandem axles, referring the position of each axle to the position of the driver axle. Influence lines for the test vehicle were not the same for northbound movement as for southbound movement because the axle loads were not symmetrical about the driver axle. Hence, influence lines for moments at Sections A and B were prepared for each direction of movement. These influence lines are shown in Figures 9 through 12. In each case there is a peak value when the driver axle is over the center of the span and another peak when the tandem axle is over the center of the span.

Experimental Moments

Since moments were not measured directly, the term experimental moment refers to the moment computed from the measured strains. These strains were converted to stresses in the initial data reduction, and all subsequent computations were based on these stresses. Computations for the experimental moments were based on the following assumptions:

1. There is an unknown amount of composite action between the slab and the steel beams.
2. There is no net axial force in the semi-composite section.
3. The slab and the steel beam always remain in contact, even though the slab may slide longitudinally on the beam (the curvature of the slab must be equal to the curvature of the steel beam).
4. The stress distributions on both the slab and the beam are linear with depth.

Assumptions 1 and 4 result in a stress distribution across the section as shown in Figure 13a. The stresses σ_t and σ_b are extreme-fiber stresses extrapolated from the original data. The analysis is equally valid for maximum or mean stresses. The stress distribution in the steel beam and the slab may be broken into axial and flexural components (Fig. 13b). From these stresses, both the axial force P and the bending moment in the steel beam M_S can be computed as follows:

$$P = \frac{\sigma_b + \sigma_t}{2} A_S \tag{1a}$$

and

$$M_S = \frac{\sigma_b - \sigma_t}{d} I_S \tag{1b}$$

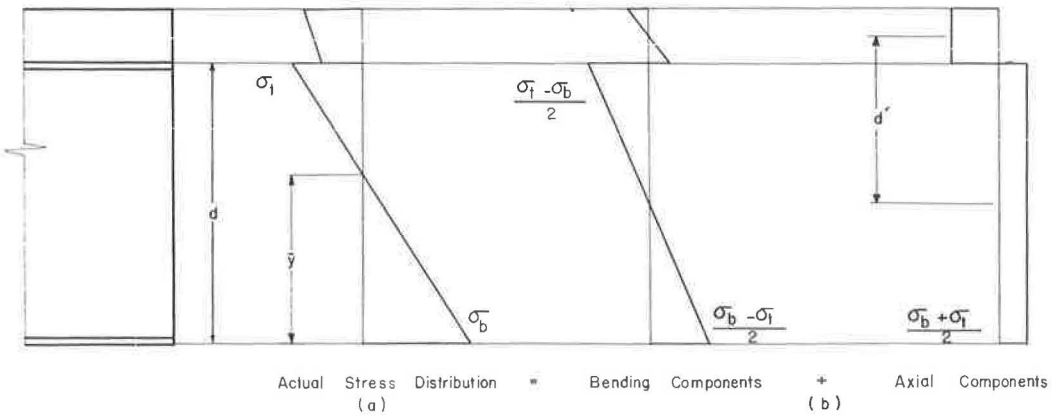

$$\text{Total Moment} = M_{(\text{steel beam})} + M_{(\text{axial force})} + M_{(\text{slab})}$$

$$M = \frac{(\sigma_b - \sigma_t)}{d} I_s + \frac{(\sigma_b + \sigma_t)}{2} A_s d' + \frac{(\sigma_b - \sigma_t)}{d} \frac{I_c}{n}$$

Figure 13. Stress distribution on semi-composite section.

where A_s is the cross-sectional area of the I-beam, I_s is the moment of inertia of the I-beam, and d is the depth of the I-beam. To satisfy Assumption 2, the axial force in the slab must be equal in magnitude and opposite in sign to the axial force in the steel beam. Hence, moment due to composite action may be computed as follows:

$$M_P = Pd' = \frac{\sigma_b + \sigma_t}{2} A_s d' \tag{2}$$

where d′ is the distance between the centroid of the slab and that of the I-beam. The only remaining bending component in the section is that in the slab itself. On the basis of Assumption 3, the moment in the slab may be computed by estimating its flexural rigidity and multiplying by the curvature of the beam. The flexural rigidity of the slab R may be expressed as

$$R = E_c I_c \tag{3}$$

where E_c is the modulus of elasticity of the concrete, and I_c is the moment of inertia of the transformed uncracked section of the slab. The curvature of the beam K may be expressed as

$$K = \frac{\sigma_b - \sigma_t}{E_s d} \tag{4}$$

where E_s is the modulus of elasticity of the steel. Hence, the moment in the slab M_c may be expressed as

$$M_c = RK = \frac{\sigma_b - \sigma_t}{d} \frac{I_c}{n} \tag{5}$$

where n is the modular ratio.

The accuracy of this last calculation may be questioned because of the uncertainties involved in determining both the effective width of the slab and the value of the modular ratio. However, calculations show that for the particular bridge in question, the moment in the slab can never exceed 4 percent of the total moment in the composite section. Thus, rather large errors in this particular component of the bending moment would result in only small changes in the total moment. The total experimental moment in the stringer M was calculated as the sum of the three components:

$$M = \frac{\sigma_b - \sigma_t}{d} I_s + \frac{\sigma_b + \sigma_t}{2} A_s d' + \frac{(\sigma_b - \sigma_t)}{d} \frac{I_c}{n} \tag{6}$$

Experimental moments were computed at Sections A and B of each stringer for each of the critical conditions.

Adding the experimental moments in the four stringers at a given section results in the total bending moment in the entire cross-section of the bridge at a particular instant. Under dynamic loading conditions this computed total is slightly in error because the moments computed for the individual stringers did not occur at exactly the same instant. Figures 9 through 12 show comparisons of the static experimental moments with the theoretical influence lines. In Figures 14 through 17, the dynamic experimental moments are compared with the theoretical values. The vertical bars

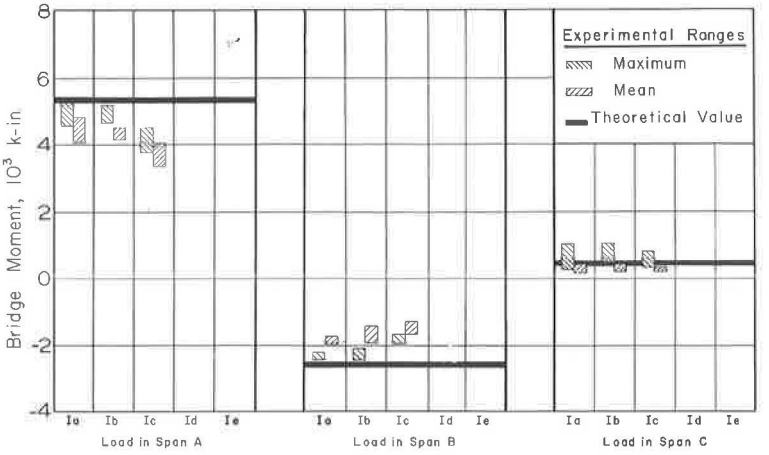

Figure 14. Dynamic ranges of bridge moment at Section A, truck northbound.

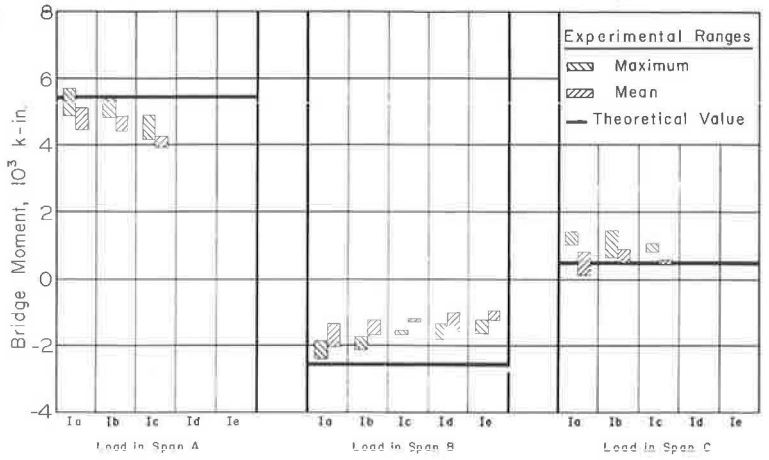

Figure 15. Dynamic ranges of bridge moment at Section A, truck southbound.

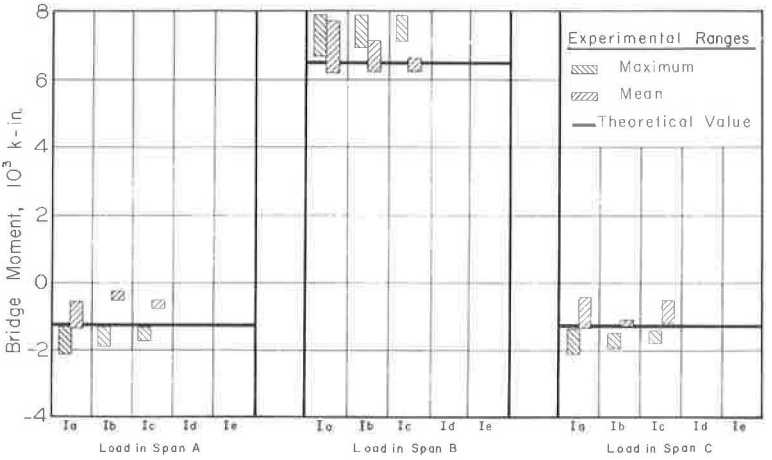

Figure 16. Dynamic ranges of bridge moment at Section B, truck northbound.

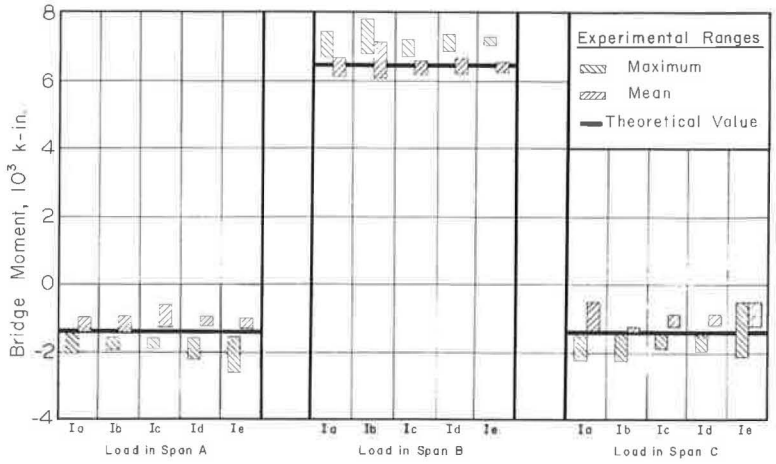

Figure 17. Dynamic ranges of bridge moment at Section B, truck southbound.

represent the ranges of total mean moments in the bridge whereas the heavy horizontal lines represent the peak values from the theoretical influence lines. The location of the truck at the time the peak moments occurred was not recorded.

In general, there is fair agreement between the experimental values and the theoretical influence lines. The static values at Section A with Span A loaded are approximately 15 percent lower than those predicted by the theory. It will be shown that the composite action in Span A was not as complete as in Span B; hence, the relative stiffness of Span A was actually less than that assumed in the analysis. This was probably the cause of the discrepancy.

The static moments at Section B from Series 1a southbound are in almost perfect agreement with the theoretical curve. The static moments at Section B from Series 1b southbound appear to be shifted approximately 1200 kip-in. in the positive direction. This shift is nearly constant for all points regardless of the span in which the truck was located and, therefore suggests some sort of a zero shift in the experimental data. One might immediately suspect such a shift in the gage readings, but more careful consideration reveals that several gage readings were incorporated in finding each of the moments plotted. None of these gage readings appear to be inconsistent with the rest of the gage readings, and it seems rather unlikely that there would be an accidental zero shift of about the same percentage in each of eight gages.

Another possible explanation of this shift is that there was a residual moment in the I-beam at the time the zero readings were taken. This residual could come about because of the friction between the slab and the steel beams. Mechanisms containing friction links normally have more than one equilibrium position. There is no proof of the cause of this apparent zero shift, but it seems to be inherent in the behavior of the bridge. This phenomenon is also present in the static runs of Series 1a and 1b northbound. The dynamic values seem to be in better agreement with the theory than the static values.

Theoretical Deflections

Elastic theory was used to prepare influence lines for deflections at Sections A and B due to a unit load passing across the bridge. This was done for both interior and exterior stringers and for both composite and non-composite action. A slab width of 80 in. and a modular ratio of 10 were used in computing the transformed section for composite action. The ordinates of the influence lines for interior and exterior stringers never differed more than 8 percent. By averaging the ordinates of these two influence lines, an influence line representing the average deflection of the four stringers was

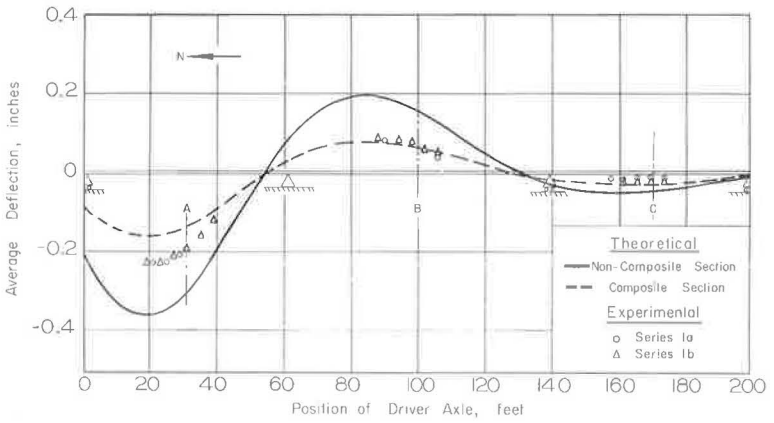

Figure 18. Influence lines for average deflection at Section A, truck northbound.

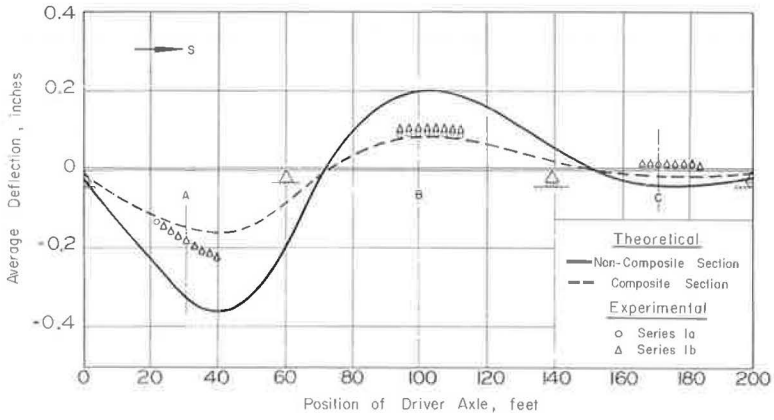

Figure 19. Influence lines for average deflection at Section A, truck southbound.

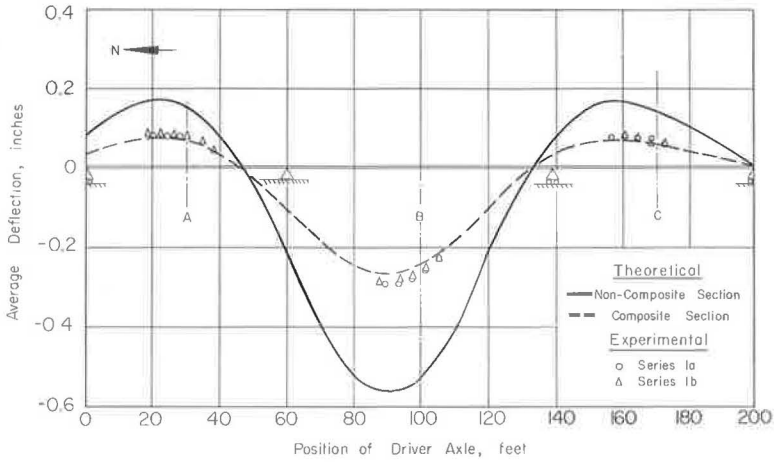

Figure 20. Influence lines for average deflection at Section B, truck northbound.

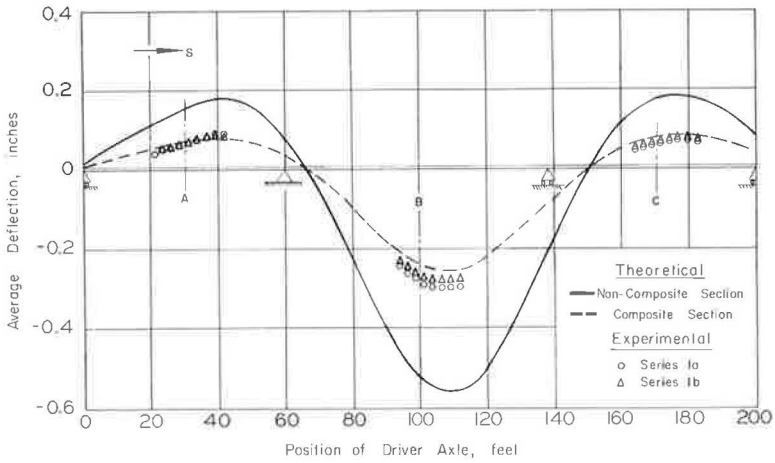

Figure 21. Influence lines for average deflection at Section B, truck southbound.

prepared. The procedure explained previously for preparing moment influence lines was then followed in preparing influence lines for average deflection due to the test vehicle. The resulting influence lines for the average deflection in the four stringers are shown in Figures 18 through 21. The solid line represents the deflections computed on the basis of non-composite action and the dashed line represents the deflections computed on the basis of composite action.

Experimental Deflections

Experimental deflections for the four stringers were averaged at each section for each critical condition. These average static deflections are compared with the theoretical values in Figures 18 through 21. Ranges of values for average deflection under dynamic loadings are compared with theoretical values in Figures 22 through 25. The position of the truck on the bridge at the time of the critical deflection was not recorded for these runs.

The static experimental deflections at Section B agree very well with the influence line for completely composite action. The deflections at Section A are somewhat greater

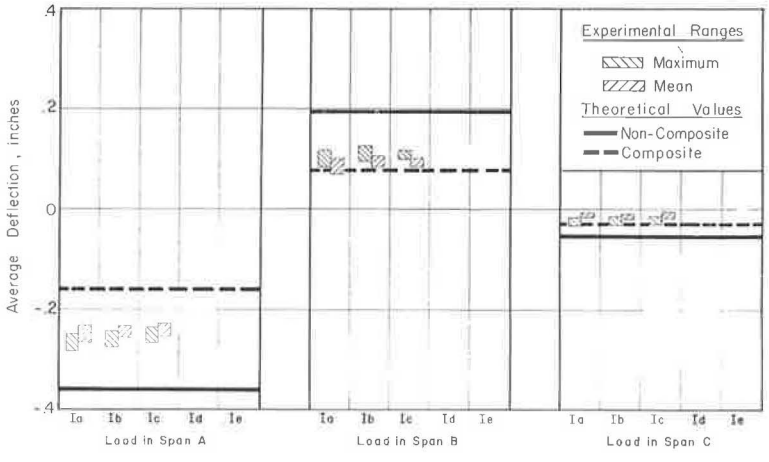

Figure 22. Dynamic ranges of average deflection at Section A, truck northbound.

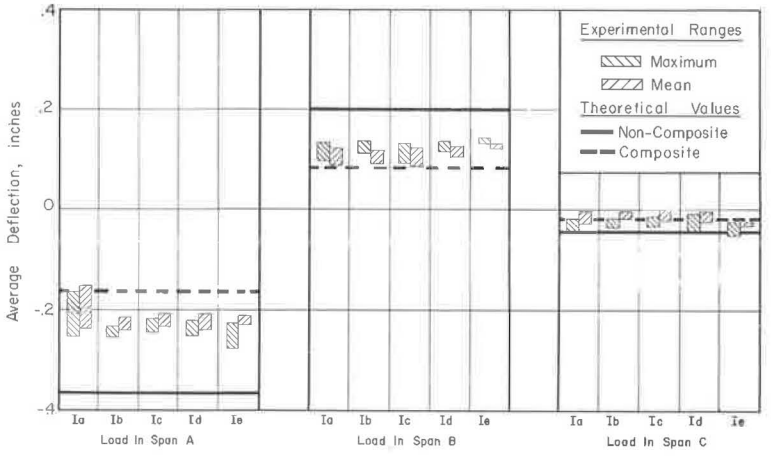

Figure 23. Dynamic ranges of average deflection at Section A, truck southbound.

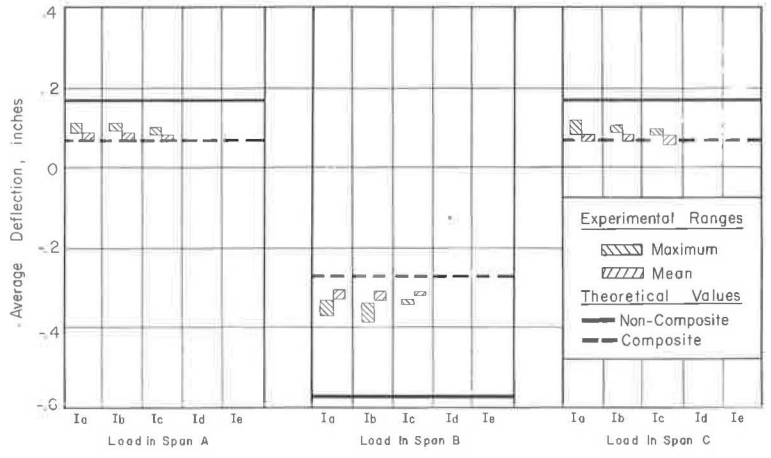

Figure 24. Dynamic ranges of average deflection at Section B, truck northbound.

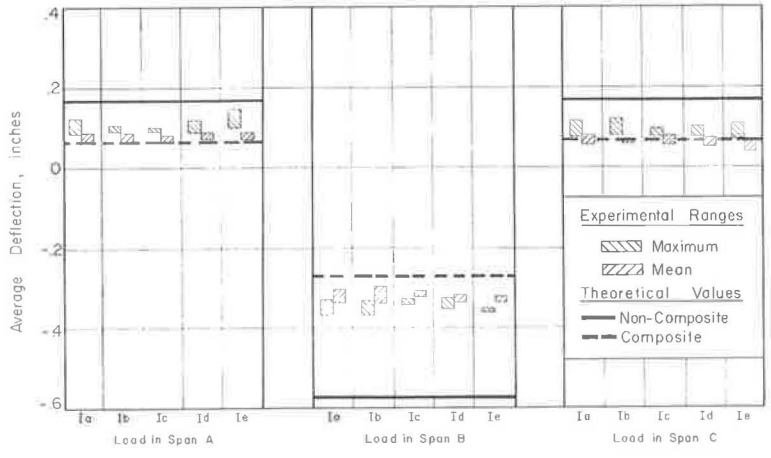

Figure 25. Dynamic ranges of average deflection at Section B, truck southbound.

than those predicted on the basis of completely composite action. This observation is further evidence that the degree of composite action was greater in the center span than in the end spans.

Figure 19 shows that the deflections at Section A were opposite in sign to those predicted by the theory when the truck was in Span C. This was probably another manifestation of the multiple-equilibrium position phenomenon of the system with a friction link. In this case the truck was southbound and had just left Span B. Thus, the deflections in Span A were changing from positive to negative. As shown in Figure 18, the deflections were in much better agreement with the theory when the truck was northbound. This phenomenon is not so noticeable in cases where the load was in Span A or B and the deflections due to load were of a much greater magnitude. In all cases the dynamic deflections were somewhat greater than the static deflections. Even so, there was still a high degree of composite action.

Moment vs Speed

To find the extent to which the impact factor was dependent on the speed of the vehicle crossing the bridge, some value on which to base the calculations had to be found. Static values were not considered desirable for this purpose because of the tendency for zero shift as indicated by the influence lines for static moment. Consequently, normalized moments based on mean stresses were plotted vs speed. The ordinate of this plot was normalized by dividing each moment value by the average of the 5-mph values for the same series, the same stringer, the same section, and the same loading conditions except for speed. By normalizing the moment values in this manner, it was possible to plot all available mean moments on a single plot (Fig. 26). A least-mean-squares fit of a straight line to all points shown in Figure 26 results in the following expression:

$$\frac{M_{mean}}{M_{mean_5}} = 1.01 - 0.000410 \times \text{speed (mph)} \qquad (7a)$$

Although there is some scatter in the data, this plot indicates that the mean moment was essentially independent of speed. This is basically in agreement with the assumptions of other investigators (2, 3, 4, 5, 6, 7). On the basis of this finding it was decided that impact was a result solely of the vibration in the bridge and that the average of the

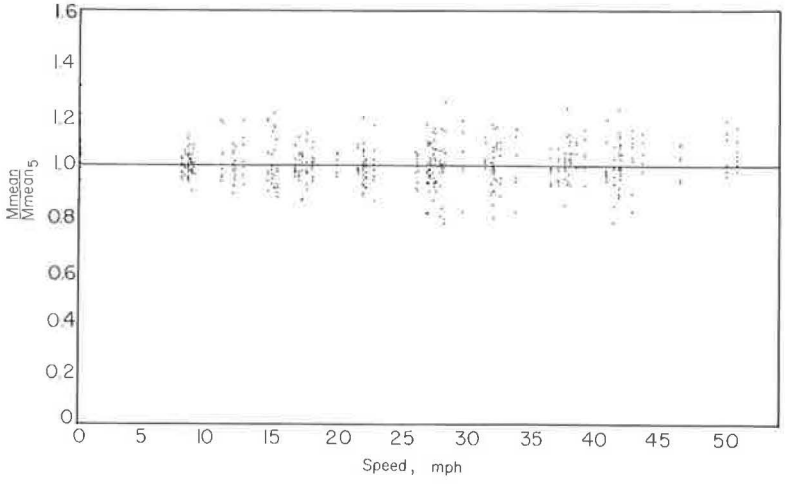

Figure 26. Normalized mean moment vs speed.

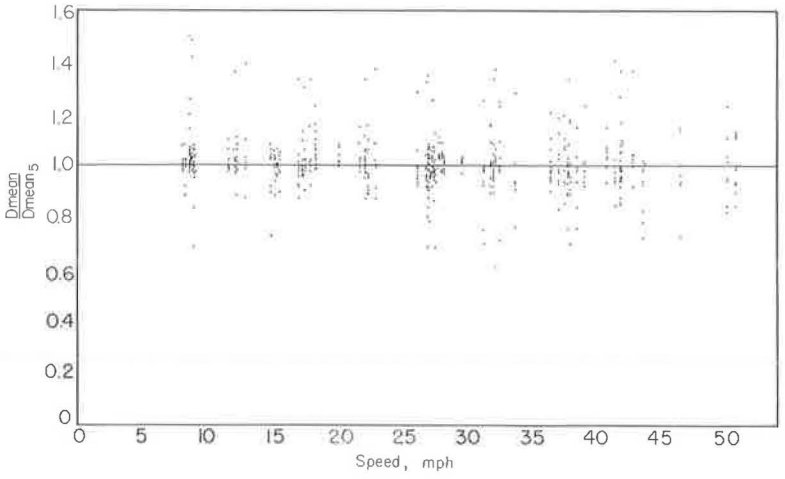

Figure 27. Normalized mean deflection vs speed.

corresponding mean moments was probably the best base value for determining impact factors.

Deflection vs Speed

In investigating the extent to which deflection was dependent on the speed of the vehicle, essentially the same procedure was followed as for moment. Each mean deflection was normalized by dividing it by the average of the corresponding deflections at 5 mph. Figure 27 was then prepared by plotting these normalized values of deflection against the speed of the vehicle, and the straight line shown represents a least-mean-squares fit. The equation of this line is:

$$\frac{D_{mean}}{D_{mean_5}} = 1.02 - 0.000327 \times \text{speed (mph)} \qquad (7b)$$

This expression again indicates that impact was due solely to the vibration of the bridge and the average of the mean values was probably the best base value for computing impact factors.

Lateral Distribution

Lateral distribution of the load was investigated by expressing the moment in each stringer as a percentage of the total moment in the section. These percentages for both static and dynamic runs are shown graphically in Figures 28 and 29. The ordinate of each of these plots represents the percentage of the total moment in the bridge section carried by each of the stringers, while the abscissa represents the four stringers of the bridge. The experimental data are represented by a band indicating the spread of values for all runs in a given series in both directions. The average values are very close to the center of the band in most cases.

The first plot in each line represents the distribution of moment in the bridge when the load was in the same span as the gages. Thus, the band designated "Gages in Span A" represents the distribution of moment in Span A when the load was in Span A, whereas the band designated "Gages in Span B" represents the distribution of moment in Span B when the load was in Span B. The second plot in each line represents the distribution of moment at the center of a given span when the load was in the adjacent span. Thus,

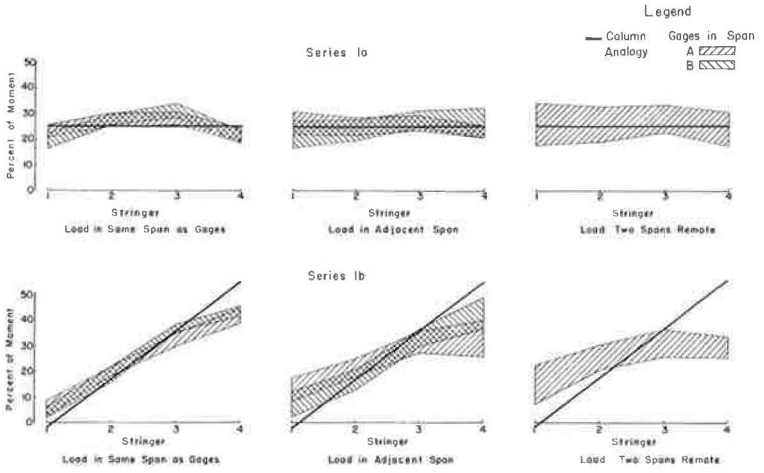

Figure 28. Lateral distribution of moment, Series 1a and 1b.

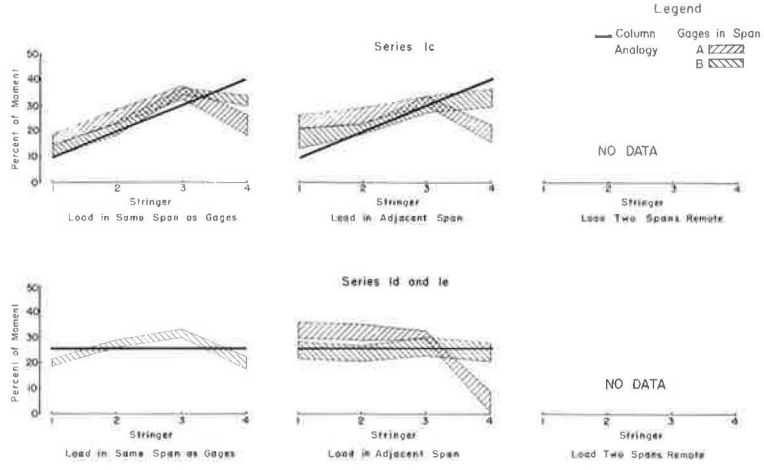

Figure 29. Lateral distribution of moment, Series 1c, 1d, and 1e.

the band designated "Gages in Span A" represents the distribution of moment in Span A when the load was in Span B, whereas the band designated "Gages in Span B" represents the distribution of moment in Span B when the load was either in Span A or Span C. Because these data were essentially the same whether the load was in Span A or Span C, the data were all indicated in a single band. The third plot in each line represents the distribution of moment in Span A when the load was in Span C. This was the only condition under which moment was measured in a span when the load was two spans remote from the gages. Malfunctioning of a few gages accounts for the missing plots in Series 1c, 1d, and 1e. The gages which did not function properly were on Stringer 4 in Span A. This difficulty may also account for the unusually low values for Stringer 4 in Span A of Series 1c, 1d, and 1e.

The most elementary of the theories for lateral distribution is based on the assumption of simple-beam action in the slab. The inaccuracy of this theory is obvious from inspection. Such a behavior would result in all the load being carried by the 2 interior

stringers for Series 1a, 1d, and 1e. For Series 1b, 97 percent of the load would be carried by Stringers 3 and 4.

A form of column analogy suggested by Prentzas (8) gives a reasonably satisfactory prediction of the lateral distribution. This method predicts the load L_i carried by ith Stringer from the formula:

$$L_i = L_t \frac{I_i}{\sum_k I_k} + L_t e \frac{y_i I_i}{\sum y_k^2 I_k} \tag{8}$$

where L_t is the load on the bridge, I_i and I_k are the moments of inertia of the ith and kth Stringers, y_i and y_k are the lateral distances from the center line of the bridge to

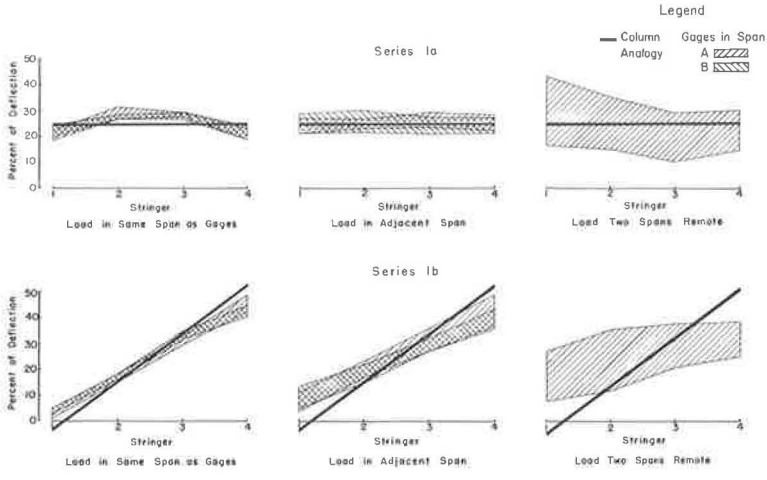

Figure 30. Lateral distribution of deflection, Series 1a and 1b.

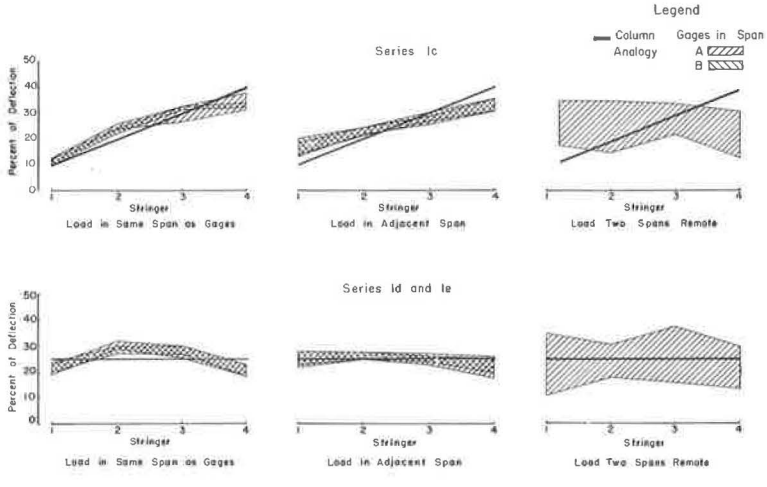

Figure 31. Lateral distribution of deflection, Series 1c, 1d, and 1e.

the i th and k th Stringers, and e is the lateral distance from the centerline of the bridge to the load (Figs. 28 and 29).

The portion of the current AASHO specifications relating to lateral distribution was developed on the basis of the work of Newmark and Siess (9, 10, 11). If one considers the effect of two trucks on the bridge by using the principle of superposition, the data agree reasonably well with these specifications. The code states that an interior stringer of the bridge under consideration should be designed for 1.21 wheel loads. Superimposing suitable data from Series 1b and 1c of the test results gives a range of 0.94 to 1.32 or an average of 1.14 wheel loads for an interior stringer. For an exterior stringer of the bridge under consideration, the code requires 1.18 wheel loads for design. Superimposing suitable data from Series 1b and 1c of the test data results in a range of 0.94 to 1.28 or an average of 1.11 wheel loads for an exterior stringer.

Lateral distribution was also investigated by comparing the deflections of individual stringers. The percent of deflection in a stringer was calculated as the deflection in the stringer divided by the sum of the deflections of the four stringers at the particular section. Figures 30 and 31 are identical to Figures 28 and 29 except that they represent the lateral distribution of deflections. This distribution was essentially the same as that for moment except for Stringer 4 of Series 1c, 1d, and 1e. This difference was undoubtedly due to some difficulty with the strain gages at Section A of Stringer 4. The comparison of the theoretical to experimental distribution of moments applies equally well to deflections.

The scatter of the data where the load was two spans remote from the gages may be explained by the very small gage readings under these conditions. With such small readings, the noise level in the instrumentation was a very large percentage of the measured quantity. There seemed to be a slight tendency for the distribution to become more uniform as the load moved farther from the section at which the moment was being measured.

Composite Action

The semi-composite action of the bridge was evaluated quantitatively on the basis of an effective section modulus. This modulus was calculated by dividing the experimental moment in a stringer by the stress in the bottom fiber. It should be noted that although the moment of inertia for a completely composite section is nearly twice as great as that for the same section with non-composite action, the effective section modulus is only 50 percent greater. The section modulus for a completely non-composite stringer in this bridge is approximately 400 cu in., whereas the section modulus for a completely composite stringer in this bridge is approximately 600 cu in.

Distributions of values of effective modulus are shown in Figures 32 and 33. The distributions calculated on the basis of mean values (Fig. 32) are essentially the same as the distributions calculated on the basis of maximum values (Fig. 33). However, the distributions of values for Span A are considerably different from the distributions of values for Span B. The values range from 400 to 540 for Span A and from 520 to 620 for Span B. Thus, the composite action was approximately 30 percent complete in Span A but more than 80 percent complete in Span B. These data are in agreement with the data for moments and deflections discussed previously. As mentioned before, the apparent reason for the much lower degree of composite action in Span A is the smaller surface over which the friction can develop composite action. This suggests that in long multispan bridges, completely composite action might be realized by placing shear developers in the end spans only. This hypothesis is purely conjecture and is intended only as a suggestion for future research.

Frequency of Vibration

The theoretical nature frequency for the fundamental mode of vibration of the bridge was calculated using the method developed by Darnley (12). This method for finding the natural frequency of multispan beams, with constant cross-section and uniformly distributed mass, results in the solution of the following equation:

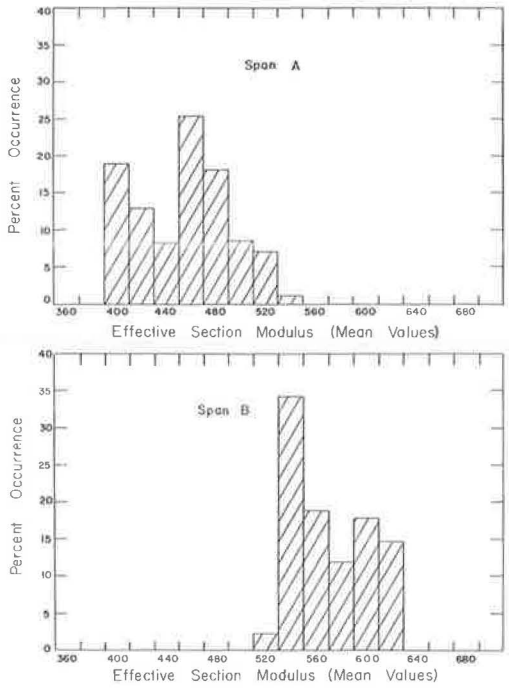

Figure 32. Distribution of values for effective section modulus (mean).

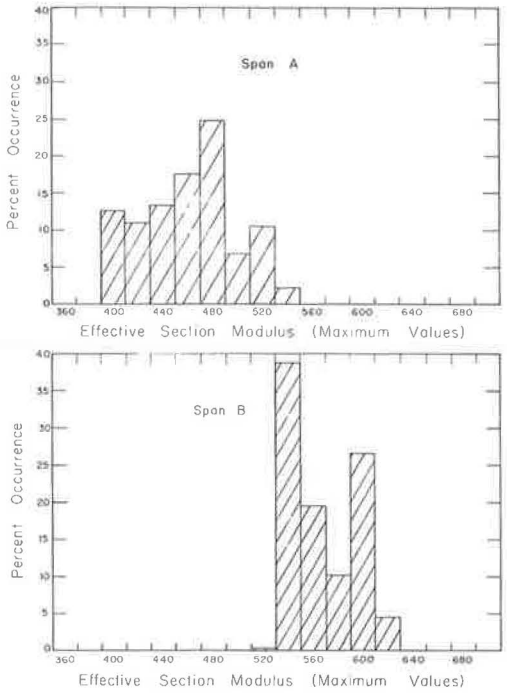

Figure 33. Distribution of values for effective section modulus (maximum).

$$F_1 = \frac{(k_1 L_1)^2}{2\pi L_I^2} \sqrt{\frac{EI_g}{w}} \tag{9}$$

where $k_1 L_1$ is the smallest root of the equation

$$\phi_1 + \phi_2 = \psi 2 \tag{10}$$

where

ϕ_r = Coth kL_r - cot kL_r,
ψ_r = Csch kL_r - csc kL_r,
L_r = length of the r th span,
E = modulus of elasticity,
I = moment of inertia of bridge,
w = weight per unit length of bridge, and
g = acceleration of gravity.

Although the moment of inertia of the bridge under investigation varied as much as 15 percent from one cross-section to another, it was decided that calculations for a constant cross-section, based on an average of the cross-sections for the bridge would be suitable. The completely composite section was expected to give the best prediction of natural frequency because of the high degree of composite action indicated by the moment analysis. The following quantities were used in the calculation:

$E = 30 \times 10^6$ psi,
$I = 64,969$ in.^{4},
$L_1 = 720$ in.,
$L_2 = 960$ in.,
$g = 386$ in./sec^2, and
$w = 243.5$ lb/in.

Using these values, the natural frequency was found to be 4.00 cycles/sec. Considering non-composite action with an I of 32,332 in.^{4} resulted in a calculated natural frequency of 2.82 cycles/sec.

The natural frequency of the bridge as determined from the oscillograph records varied from 4 to 4.9 cycles/sec with an average of about 4.2 cycles/sec. There seemed to be no perceptible difference between the natural frequencies under loaded and unloaded conditions, which agreed with the analysis. Consideration of the weight of the truck distributed over the entire length of the bridge would have changed the calculated natural frequency by only 3.3 percent.

Amplitude of Vibration

According to the findings of Hayes et al. (3), one might expect some degree of resonance at speeds of 11.5, 36.6, and 53.4 mph by considering the distance between the two tandem axles, between the front axle and the driver axle, and between the driver axle and the first of the tandem axles. This resonance would result in substantial increases in the amplification factor at these speeds.

The amplification factor may be defined as the ratio of the maximum moment, stress, or deflection to the mean moment, stress, or deflection. It follows from the previous discussions that the impact factor IF may be computed from this amplification factor as follows:

$$IF = \text{amplification factor} - 1 \tag{11}$$

Impact factors were computed on the basis of both moment and deflection for each of the sets of critical values. The impact factor IF_M based on moment was computed from the equation

$$IF_M = \frac{M_m - M_a}{M_a} \tag{12}$$

where M_m is the maximum moment and M_a is the average of all the corresponding mean moments. The impact factor IF_D based on deflection was computed from the equation

$$IF_D = \frac{D_m - D_a}{D_a} \tag{13}$$

where D_m is the maximum deflection and D_a is the average of all the corresponding mean deflections.

The impact factors at each nominal speed were averaged and these were plotted against speed in Figure 34. This graph indicates no significant increase in the impact factor at speeds of 11.5 or 36.6 mph. There is some indication that the impact factor was increasing as the 53.4-mph speed was approached. Unfortunately, the greatest nominal test speed was 50 mph. The lack of sensitivity to the repeated loads applied by the tandem axles might be expected because of the extremely short distance between the two axles. Lack of sensitivity to repeated loads applied by the front axle and the driver axle might be attributed to the low load on the front axle.

Figure 35 shows the distributions of impact factors at all speeds. The peak of the distribution curve for impact factors based on moment falls between 0.10 and 0.12,

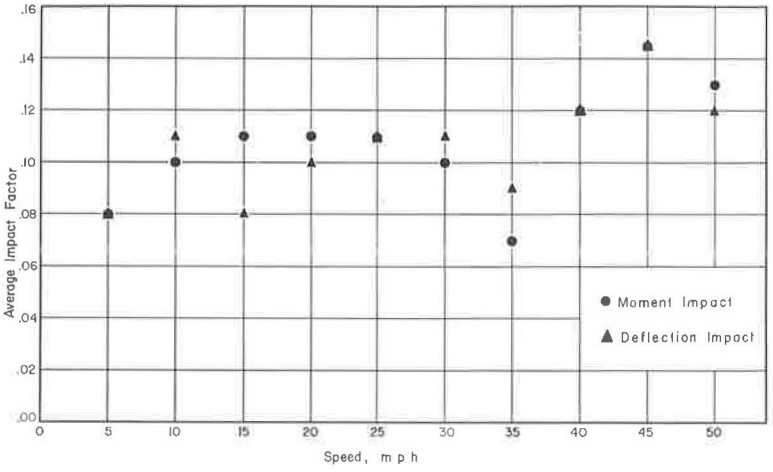

Figure 34. Average impact vs speed.

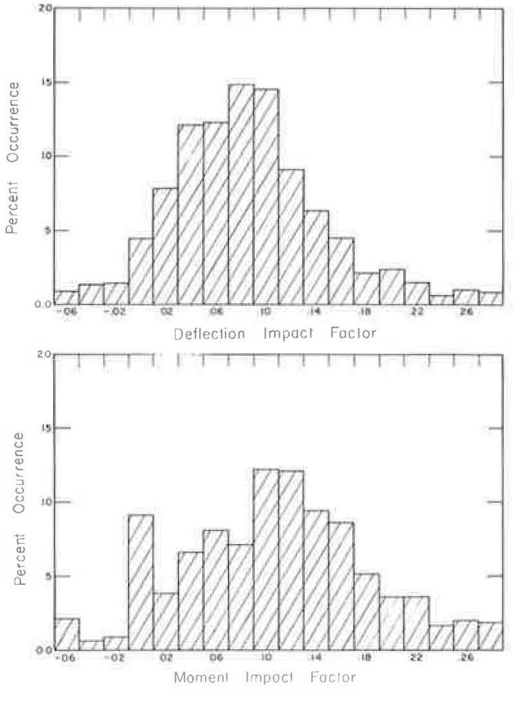

Figure 35. Distribution of impact factors.

whereas the peak of the distribution curve for impact factor based on deflection falls between 0.08 and 0.10. One might expect impact factors for moment to be slightly greater than those for deflection because the moment is a local condition and the deflection is an integral of the moments over the length of the span. Although the peaks of the distribution curves are considerably less than the values of 0.238 and 0.27 required by AASHO specifications for the bridge under investigation, there is a great deal of scatter in the data with some values more than twice the mean value. For this particular set of tests, 96.5 percent of the impact factors fell below the 0.25 level. Thus, one might well consider the currently accepted design impact factor as a suitable and conservative limit.

Induced Roughness

Series 1d and 1e of the test program were conducted to determine the effect of induced roughness at the bridge approach on the impact factor. The data indicate no significant increase in the impact factors for Series 1d and 1e. An examination of the records taken from the axle housings of the truck revealed such great damping of the suspension system of the truck that the initial oscillations produced by the induced roughness were damped out in approximately 1 to 1½ cycles. The time required for these oscillations to be damped out was much less than the time required for the truck to move from the approach to the center of the span. Therefore, the high forces produced by these initial oscillations were not applied to the bridge at a location that would produce large moments in the bridge.

SUMMARY AND CONCLUSIONS

Data from the five series of tests outlined in Table 1 were analyzed and compared with existing theories and design codes. Mean moments in the test structure were calculated from the observed strains and compared with the moments predicted by elastic theory. These comparisons were generally in good agreement. The greatest discrepancies occurred in the static data and were presumably the result of the multiple-equilibrium positions of the bridge, a result of the friction link between the slab and the steel I-beam.

The average experimental deflection at each section in the bridge for each series of tests was compared with the average deflection calculated on the basis of elastic theory for both composite and non-composite action. The actual behavior of the structure was much closer to completely composite action than to non-composite action. The deflections in the center span were almost identical to those predicted on the basis of completely composite action, whereas the deflections in the end span were approximately $\frac{1}{3}$ of the way between completely composite and non-composite action.

Mean moments and mean deflections were found to be essentially independent of speed. This indicated that the effect of impact on the bridge was entirely due to the vibrations of the bridge. Hence, moment impact factors were calculated as the difference between the maximum and the mean moments divided by the average of the corresponding mean moments. Deflection impact factors were calculated in the same manner. A plot of these impact factors against speed shows that the impact factor was independent of speed for speeds less than about 40 mph. Some indication exists that the impact factor was increasing beyond that speed, but no data are available beyond 50 mph. Assuming that the period of time between the passage of two wheels over a given point of the bridge may be treated as the period of a repeated forcing function on the bridge, and considering the measured natural frequency of vibration of the bridge, one might predict that a resonance would be reached at a speed of approximately 55 mph. The lateral position of the truck on the bridge seemed to have little effect on the impact factors.

The measured natural frequency of the bridge was approximately 5 percent greater than that predicted by Darnley's analysis (12) considering completely composite action.

The lateral distributions of moments and deflections were compared with an analysis suggested by Prentzas (8) and also with the AASHO code. Both of these comparisons showed reasonable agreement. However, comparison with the code required using superposition, a procedure subject to some criticism. Computing lateral distribution on the basis of simple beam action in the slab resulted in very poor agreement with the test results.

An analysis of the amount of composite action based on an effective section modulus revealed essentially the same information as the comparison of deflections. The section modulus in the center span was nearly equal to that of a completely composite section. The amount of composite action in the end span was approximately 30 percent. This difference perhaps was due to the difference in the amount of surface between the slab and the I-beam available for the development of composite action. In the end span, the surface available to develop the composite action through friction was limited to the surface between the center and end of the span, whereas in the case of the center span the surface available for developing composite action extended from the center of the center span through the entire length of the end span.

The test results indicated that induced roughness at the approach of the bridge had little or no effect on the maximum moments observed in the bridge. The oscillations of the truck induced by roughness at the approach were damped out before the truck reached a position on the bridge which would produce large moments.

The observed behavior of the structure was not materially different from that predicted by current theory and design codes. The idea of an impact factor to account for the effects of dynamic loading is rather crude and does not take into account the possibility of resonant vibration. However, present specifications were reasonable for the design of this particular bridge under the particular loading conditions of this investigation. This might not have been the case if the test runs had continued to slightly higher speeds.

Continuous Span vs Simple Span

There were two significant differences between the simple and continuous spans. The 45-ft simple span was only 75 percent as long as the shortest of the continuous spans. The mass of the simple span was approximately 25 percent as great as the mass of the combined continuous spans.

Both stresses and deflection indicate that there was much less composite action in the simple span than in the continuous spans. This may be accounted for in the same manner as the difference in composite action between continuous Spans A and B. Much less surface was available in the short simple span to develop the composite action through friction.

Impact factors for the simple span were slightly higher than those for the continuous spans. This might be expected because of the span length and, in fact, is indicated by the code provisions. Impact factors for the simple span seem to be somewhat more dependent on the speed and direction of the vehicle than are those for continuous spans. This may be an indication that the simple span was much more sensitive to the oscillations of the truck. The ratio of the mass of the truck to the mass of the structure was much higher for the simple span than for the continuous spans. The short span length also made it possible for the truck to reach the center of the bridge before the oscillations of the vehicle were damped out. Induced roughness caused significant increases in the impact factors for the simple span, which was not true for the continuous spans.

The frequency of free vibration of the unloaded simple span was observed to be 9 cycles/sec. The calculated natural frequency for the unloaded simple span, based on completely composite action and a modular ratio of 10 for the concrete, was 7.12 cycles/sec. The observed frequency of the loaded simple span was 8 cycles/sec, whereas the calculated natural frequency for the loaded simple span was 5.76 cycles/sec. Differences between the calculated and observed natural frequencies of the simple span were considerably greater than those for the continuous spans. This may have been due in part to the sensitivity of the bridge to the oscillations of the truck.

During creep runs the simple span was observed to vibrate at a frequency of 3.5 cycles/sec. This is in fairly close agreement with the calculated value of 3.61 cycles/sec for the loaded simple span if it were behaving in a completely noncomposite manner. The lateral distributions of both moment and deflection in the simple span and in the continuous spans were essentially the same.

REFERENCES

1. Impact Study of a Simple I-Beam Span of a Highway Bridge. Missouri State Highway Department, Div. of Bridges, 1958.
2. Biggs, John M., and Suer, Herbert S. Vibration Measurements on Simple Span Bridges. Highway Research Board Bull. 124, pp. 1-15, 1955.
3. Hayes, John M., and Sbarounis, John A. Vibration Study of Three-Span Continuous I-Beam Bridge. Highway Research Board Bull. 124, pp. 47-78, 1955.
4. Edgerton, Roy C., and Beecroft, Gordon W. Dynamic Studies of Two Continuous Plate-Girder Bridges. Highway Research Board Bull. 124, pp. 33-46, 1955.
5. Scheffey, Charles F. Dynamic Load Analysis and Design of Highway Bridges. Highway Research Board Bull. 124, pp. 16-32, 1955.
6. Foster, George M., and Oehler, Leroy T. Vibration and Deflection of Rolled-Beam and Plate-Girder Bridges. Highway Research Board Bull. 124, pp. 79-110, 1955.
7. Fenves, S. J., Veletsos, A. S., and Siess, C. P. Dynamic Studies of Bridges on the AASHO Test Road. Univ. of Illinois, Civil Eng. Studies, Structural Res. Ser. No. 227, 1962.
8. Prentzas, Elias George. Dynamic Behavior of Two Continuous I-Beam Bridges. Iowa State Highway Commission, Material Dept., 1958.
9. Newmark, N. M. A Distribution Procedure for the Analysis of Slabs Continuous over Flexible Beams. Univ. of Illinois, Exper. Sta., Bull. 304, 1938.
10. Newmark, N. M., and Siess, C. P. Moments in I/Beam Bridges. Univ. of Illinois, Exper. Sta., Bull. 336, 1942.

11. Newmark, N. M. Design of I-Beam Bridges. Trans. ASCE, Vol. 114, pp. 997-1022, 1949.
12. Darnley, E. R. The Transverse Vibrations of Beams and the Whirling of Shafts Supported at Intermediate Points. Phil. Mag., Vol. 41, p. 81, 1921.
13. Baldwin, J. W., Jr. Impact Study of a Steel I-Beam Highway Bridge. Univ. of Missouri, Eng. Exper. Sta., Bull. 58, 1964.